Medical Engineering and Physics 66 (2019) 26–39

Contents lists available at ScienceDirect

Medical Engineering and Physics

journal homepage: www.elsevier.com/locate/medengphy

Mucus transport and distribution by steady expiration in an idealized airway geometry

Rahul R Rajendran, Arindam Banerjee*

Department of Mechanical Engineering and Mechanics, Lehigh University, 19 Memorial Drive West, Bethlehem, PA 18015, United States

ARTICLE INFO

Article history:
Received 15 March 2018
Revised 12 December 2018
Accepted 10 February 2019

Keywords:
Mucus transport
Gas-liquid annular flow
Secondary flows
Bifurcation model

ABSTRACT

Mucus clearance from the airways is vital to reduce the risk of infection and to improve pulmonary function. The removal of mucus is propelled either by a rhythmic ciliary motion or shear-induced by turbulent expiratory airflow. However, in chronic airway diseases, the mucociliary motion is impaired due to mucus hypersecretion and altered biophysical properties. As a result, the ciliary motion is insufficient to remove mucus from the airways and expiratory airflow plays the more dominant role. In this work, the role of expiratory airflow in pathologic mucus clearance was investigated in a three-dimensional idealized bifurcating lung geometry. The two-phase air-mucus annular flow was investigated using a homogeneous flow approach and the complex interface (free-surface) was tracked by employing the volume-of-fluid (VOF) method. Flow turbulence was modeled using the $k-\omega$ shear stress transport (SST) model to examine the role of mucus viscosity, airflow rate, gravity, and airway branching on mucus distribution. It was observed that a gravity dominated eccentric core-annular flow developed in the daughter branches. The eccentricity varied with the angle of inclination, curvature, airflow rate, and mucus viscosity, which affected the merging location of airflow from the daughter branches. A mucus secondary flow developed due to the curvature in the airways and caused a local redistribution of mucus reducing the eccentricity. In addition, it was also observed that the thickness of the mucus layer was affected by the secondary airflow in the parent branch. These results emphasize the importance of accurate modeling of mucus-lined airways and indicate that an effective clearance therapy can be devised by analyzing the distribution of mucus in the airway tree.

1. Introduction

The clearance of mucus acts as the primary defense mechanism against inhaled foreign particles, thereby reducing the risk of airway infection and improving lung function [1,2]. A healthy human lung airway is lined with a mucociliary layer which is 5–10 μm thick, and consists of the mucus layer, the serous layer and the ciliated epithelium [3,4]. Mucus is a non-Newtonian fluid that exhibits shear-thinning and viscoelastic behavior and is removed from the airways by two principal mechanisms; (i) mucociliary clearance by the consistent beating of the cilia, or, (ii) interaction with the airflow generated via a cough or forced expiration [1,5,6]. Mucus clearance through the micrometric ciliary motion is impaired in acute respiratory diseases due to mucus hypersecretion and adversely altered mucus properties, such as high viscosity, elasticity, and tenacity [1,3,7]. The mucus layer grows thick due to excessive production and stasis, and its interaction with the core airflow solely determines mucus distribution, clearance and pressure drop across the airways [8,9]. Mucus viscosities under such pathologic states has been reported to be between 1–100 Pa s and their thickness could be as high as 20% of the airway diameter [5,6].

In the airways, mucus exists as an annular sleeve along the walls accompanied by the high velocity air which occupies the core [2]. Such gas-liquid annular flows are characterized by a deformable interface consisting of waves widely varying in amplitude and frequency [10,11]. Aerosol deposition experiments conducted in compliant tubes [12] and mucus-lined tubes [13] have reported increased deposition when the wavy motion of the wall or the amplitude of the interfacial waves intensified. The deposition enhancement was attributed to the oscillatory boundary layer resulting in increased turbulence and enhanced gas transport. King et al. [14] conducted experiments using a simulated cough machine and reported increased cough clearance for greater mucus depth and reduced mucus cross-link density due to the occurrence of transient waves. Kim et al. [15] identified the critical conditions for two-phase air-mucus flow mechanism to occur in a rigid tube, and the effect of mucus properties and airflow rates on the mucus layer thickness and velocity were investigated [16]. Camassa et al. [17]

* Corresponding author.
E-mail address: arb612@lehigh.edu (A. Banerjee).

https://doi.org/10.1016/j.medengphy.2019.02.006
1350-4533/

Table 1
Literature review of experimental & computational studies investigating airflow driven mucus clearance. [Abbreviations: E: Elastic; Vi: Viscous; VE: Visco-Elastic].

Author, Year	Objective	Geometry (Generation, h/D)	Mucus type: Viscosity (Pa.s)	Re_{air}
King et al. [14]	Understand effect of rheology and layer depth on clearance of mucus by cough.	G0, 0.097–0.254	VE: 0.035–0.35	22,005–48,411 (Peak)
Kim et al. [15][a], [16][b], [19][c]	Identify effect of critical flow conditions[a]; airflow rates & mucus properties[b]; asymmetric periodic flow[c] on mucus clearance by forced expiration	G0, 0.01–0.2	Vi &VE simulants: 1.3–66	849–10,028
Chang et al. [18]	Identify air-mucus interaction under high frequency oscillatory airflow.	G0, 0.157–0.254	VE gels: 0.19–0.8	26,935 (Peak)
Zahm et al. [20]	Examine the role of repetitive simulated coughing on mucus clearance.	G0, 0.157	VE gels	35,208 (Peak)
Evrensel et al.[23,22,21]	Linear stability analysis of a mucus lined rigid tube.	G0, 0.06–0.29	E & VE: 0–0.035	13–7005
Ragavan et al. [7]	Investigate mucus displacement during cough under oscillations generated by the Acapella device.	G0	VE gel aliquot: 0.07, 0.12	5460–32,759
Mauroy et al. [8]	Study the effect of geometry, physical properties of mucus and expiratory airflow on mucus clearance.	G0-G17, 0.175–0.25	VE: 0.1, 1	661–66,182
Camassa et al. [17]	Investigate mucus transport under steady airflow to identify mechanisms of mass transport.	G0, 0.05–0.35	Vi oils: 12.9, 60	2830–10,028
Satpathi et al. [48][d], Satpathi and Ramu [24][e]	Investigate mucus transport in a simulated cough machine driven by a transient pressure gradient in two-phase flow[d] and three-phase flow[e].	G0, 0.042–0.168	VE: 0.05–1 Vi sol: 0.001 - 0.01	0–37,500
Mitran [2]	Multiscale modeling of central air flow induced mucus transport.	G0-G3, 0.04	VE	4866–10,427
Paz et al. [26]	Study mucus clearance effectiveness during a transient cough cycle in a flexible realistic geometry with emphasis on the thickness, viscosity and flowrate.	Mouth-G0, 0.002–0.035	VE	0–90,000
Current Investigation	Capture complex interface of air-mucus two-phase turbulent core-annular flow and identify flow morphology; Investigate effect of mucus viscosity, expiratory airflow rate, gravity and airway branching on mucus clearance; Establish interdependence between primary and secondary flow and relative distribution of the phases.	G0-G2, 0.07–0.138	Vi: 7.9, 20	2720–6839 (sT),4522–6030 (sBi & dBi)

[a–e]Used to indicate the work done by the same group in different publications.

extended the investigation to understand the mechanism of mass transport and they demonstrated that ring waves trapped the core airflow and travelled relative to the base shear flow, serving as the dominant mode of transport. Experimental investigation of mucus clearance under periodic flow conditions have illustrated that, an expiratory bias of airflow along with a short expiration time caused a net movement of mucus towards the mouth, due to the greater shear stress induced at the air-mucus interface [18–20].

The effect of mucus thickness and its viscoelasticity on flow onset speed and wavelength was numerically investigated to understand the interaction of laminar and turbulent airflow with mucus [21–23]. Several studies have also reported that an increase in thickness and reduction in viscosity of the underlying serous layer led to enhanced mucus clearance [3,24]. The effectiveness of cough, with and without superimposed oscillations, on the clearance of viscoelastic mucus was investigated under various inclination angles [7]; higher clearance rates were observed at larger angles of inclination from horizontal, in the presence of airflow oscillations. Mauroy et al. [8] developed a model of mucus clearance with specific focus on the role of the airway tree in addition to the mucus rheology and airflow rate. Their model determined the maximum feasible mucus thickness in each branch of the bronchial tree, however, the effect of gravity, turbulence and fluid inertia were neglected, which affects the interfacial distribution of air and mucus as well as the flow structures developed. Additionally, gravitational effects could either favor or oppose mucus transport depending on the inclination of the individual channels, and different flow regimes: horizontal/inclined stratified, concentric/eccentric annular and misty flows have been reported [5,7,25]. Paz et al. [26] recently investigated the effect of mucus thickness, viscosity and airflow rate on cough clearance in a flexible oral-tracheal geometry using CFD simulations, by adopting a Eulerian wall film model to capture the transient mucus evolution. Table 1 provides a summary of the various studies that investigate airflow driven mucus transport.

The effectiveness of drug therapy depends on the distribution of mucus in the airways as it acts as both a target and a barrier for the administered medications [9,27]. We hypothesize that air-mucus interaction in the branched airways would affect both primary and secondary flow resulting in complex interfacial distribution, and that the effect of a thickened mucus layer cannot be conclusively estimated by modeling an airway wall with a reduced diameter. Furthermore, our literature review illustrates an existing knowledge gap on the effect of secondary currents in two-phase flow and a lack of subsequent characterization of the relative distribution of the phases and local flow structures similar to studies done in single-phase [25]. For this purpose, we model the two-phase air-mucus flow under steady expiration in an idealized lung geometry under a homogeneous flow approximation; the underlying assumptions are imposed to keep the geometry simple and avoid complexities in secondary flow structures that arise from patient specific models [28]. The wavy interface between the phases is tracked using a volume-of-fluid (VOF) method, and turbulence is modeled employing the $k-\omega$ shear stress transport (SST) model. The results were validated with the experimental data of Kim et al. [16]. The reported effort is the first step towards the computational modeling of airflow driven mucus transport in 3D-bifurcation geometries; providing a detailed understanding of mucus distribution

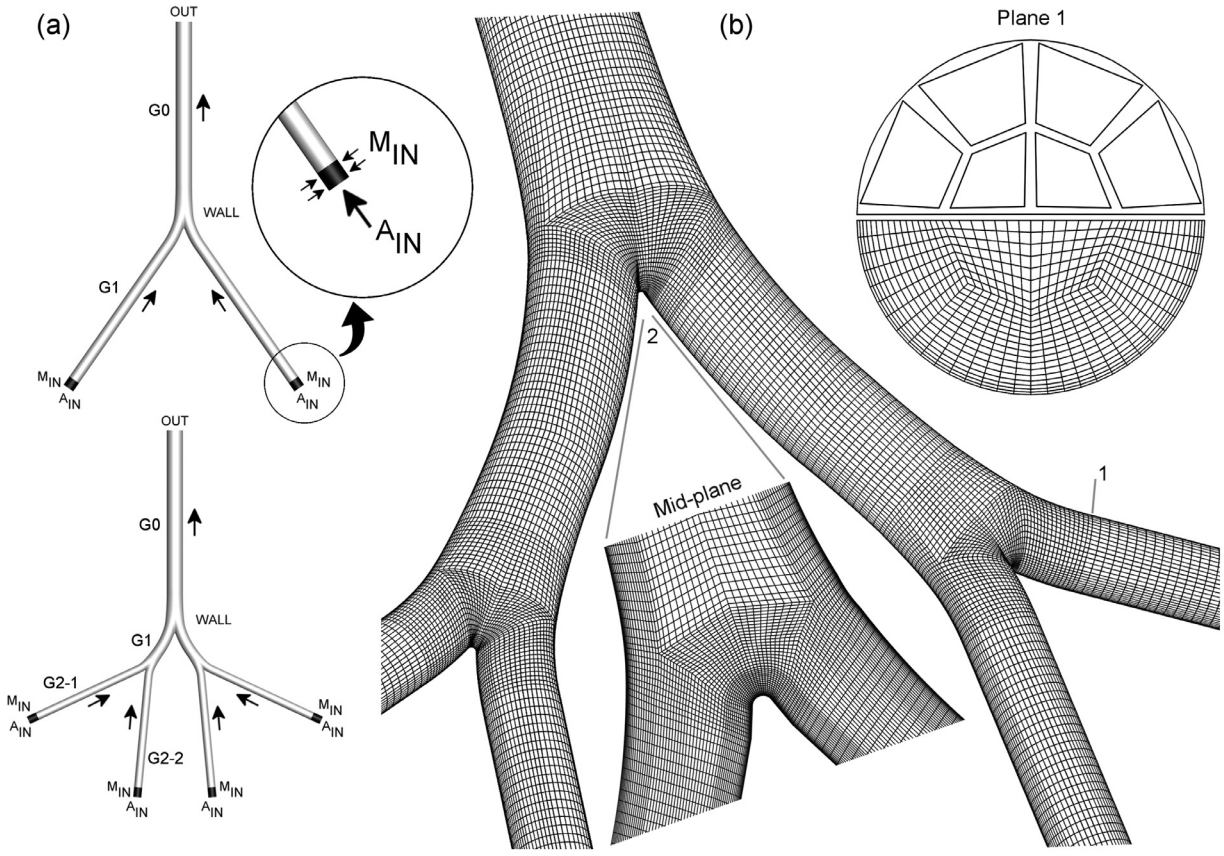

Fig. 1. Geometry and computational mesh used in the study. (a) sBi geometry (top) and dBi geometry (bottom), with a zoomed inset displaying the flow distribution at the inlets. (b) Structured hexahedral grid (medium resolution) employed for the dBi geometry, illustrating the grid at two locations: (1) Plane 1 in G2-1 branch and (2) mid-plane of the first bifurcation. A schematic of the blocking structure (2 blocks for the inner core-region and 4 blocks for the outer wall-region) at the top half, and the medium resolution grid at the bottom half are presented for Plane 1.

that could help devise better clearance therapy and drug delivery techniques.

2. Methods

2.1. Geometry and boundary conditions

Two-phase air-mucus flow was investigated in a straight tube (sT) of inner diameter of 10 mm [16] and in two simple bifurcation models: a single-bifurcation (sBi) model [29] and a double-bifurcation (dBi) model with generations G0-G1 and G0-G2, respectively. The diameter of the trachea (G0) was scaled to be 16.4 mm for the bifurcation models to match the realistic lung airway model of Alzahrany et al. [30]. The bifurcation geometries used in the current study were designed using the equations described in Zhao and Lieber [31]. Furthermore, the dBi geometry was modeled based on the dimensions of the Weibel's symmetric model [32] with a branching angle of 70° and 60° for the successive bifurcations [31,33]. The local radius of curvature (R_c) in the bifurcation models is equal to $7d_1$ for the first bifurcation [31], and $4.5d_2$ for the second bifurcation [34], where d is the diameter of the daughter tube. The carina was rounded by 0.1 times the diameter of the daughter branch to ensure smooth pathways which prevent the tearing of the mucus layer [33]. The inlet region was extended by 15 times its diameter to avoid the deviations due to air-mucus interaction at the injection region thereby ensuring that the mucus forms a uniform film [35]. Similarly, the outlet region was extended by 10 times its diameter to prevent backflow effects [29].

The interfacial shear due to a steady, unidirectional airflow is relatively constant compared to periodic airflow conditions where the direction and magnitude varies [8,16]. The mucus layer responds to this interfacial shear by an initial elastic deformation which transitions to a steady flow with constant deformation rate [16,27]. Thus, the viscoelastic mucus is reported to behave as a Newtonian liquid beyond a critical shear value [4,8], and for the steady-state conditions considered in our study, mucus was modeled as a Newtonian liquid; viscosity (μ_l) values of 7.9 Pa s (79 Poise), and 20 Pa s (200 Poise) were used to match the experimental parameters of Kim et al. [16]. To replicate the physiological secretion and transport of mucus [1,3], mucus was considered to enter the domain radially through M_{IN} (see Fig. 1a). A mass flow rate boundary condition was prescribed at M_{IN} with mucus volume fraction set to 1. To achieve a mucus layer thickness representative of airway disease [6,16], the total mucus flow rate (Q_l) for the vertical tube was maintained at 1 mL/min (1.67×10^{-5} L/s), and the bifurcation models had a flowrate of 2 mL/min (3.33×10^{-5} L/s) split equally among the inlets. Air enters through A_{IN} and drives mucus towards the trachea by interfacial shear. A fully developed velocity profile with the volume fraction of air set to 1 was imposed at A_{IN}. Four steady expiratory airflow rates (Q_{air}) were selected for the current study: 0.33 L/s and 0.5 L/s for the sT model; 0.9 L/s and 1.2 L/s for the bifurcation models. The airflow rates represent forced expiration and were chosen based on the critical airflow required for the upward transport of mucus as reported by Kim et al. [15]. A constant zero static pressure Dirichlet boundary condition was prescribed at the outlet and a stationary, no-slip boundary condition was implemented at the rigid wall [36]. The velocity/mass flow rate at the inlet and static pressure at the outlet are a well-posed set of boundary conditions and have been employed in various multiphase simulations to accurately capture the gas-liquid flow morphology [36,37]. These boundary conditions were

Table 2
Test cases with non-dimensional parameters used in the current study.

Geometry	Mucus feed rate, Q_l ($\times 10^{-5}$ L/s)	Mucus viscosity, μ_l (P)	Airflow rate, Q_{air} (L/s)	[a] Re_g	[b] Dn_1	[b] Dn_2
sT	1.67	79	0.33, 0.5, 0.83	2720, 4120, 6839	–	–
sT	1.67	200	0.33, 0.5, 0.83	2720, 4120, 6839	–	–
sBi	3.33	79	0.9, 1.2	4522, 6030	855, 1140	–
sBi	3.33	200	0.9, 1.2	4522, 6030	855, 1140	–
sBi[c]	–	–	0.9, 1.2	4522, 6030	855, 1140	–
dBi	3.33	79	0.9	4522	855	754
dBi	3.33	200	0.9	4522	855	754
dBi[c]	–	–	0.9	4522	855	754

[Abbreviations: sT - straight tube, sBi - single bifurcation, dBi - double bifurcation, ρ_g - density of air, J_g - superficial velocity of air, D_T - tracheal diameter, d - local airway diameter, R_c - local radius of curvature].

[a] Tracheal airflow Reynolds number, $Re_g = \rho_g J_g D_T/\mu_g$.

[b] Dean number at first and second bifurcation, respectively $Dn = Re\sqrt{d/2R_c}$.

[c] The dry-wall cases with no mucus lining on the walls.

inspired by the experiments conducted by Kim et al. [13,16] and Camassa et al. [17], and the ease of recreating these boundary conditions physically in the form of an experimental setup makes these boundary conditions suitable for the current investigation. The sensitivity of the numerical solution to different initial conditions was analyzed. Based on the analysis, the flow domain was initialized by setting the mucus volume fraction to 1 across all the cells [8,38]. The initial pressure condition was prescribed by setting the hydrostatic pressure gradient across the domain with the outlet as the reference location. The various test cases considered for the current investigation together with the tracheal airflow Reynolds number and the Dean number are summarized in Table 2.

2.2. Numerical methods and mesh generation

The air-mucus flow in the current study was investigated using the homogeneous multiphase model in ANSYS® CFX® software (ver. 17.0) by employing the volume-of-fluid (VOF) method [39] which is commonly used to track the position of the interface between two or more immiscible fluids on a fixed Eulerian mesh [36,40–42]. The volume fraction (α) serves as an indicator function of a specific phase and takes a value of 0 (empty) or 1 (full) and switches between 0 and 1 at the interface. The phasic continuity Eq. (1), and the bulk Reynolds-averaged continuity and momentum conservation equations for the homogenous multiphase model (2) are:

$$\frac{\partial \alpha_l}{\partial x_i} = 0 \tag{1}$$

$$\frac{\partial}{\partial x_i}\left(\rho_m \overline{\boldsymbol{U}_i}\right) = 0;$$
$$\frac{\partial}{\partial t}\left(\rho_m \overline{\boldsymbol{U}_i}\right) + \frac{\partial}{\partial x_j}\left(\rho_m \overline{\boldsymbol{U}_j}\overline{\boldsymbol{U}_i}\right) = -\frac{\partial P}{\partial x_i} + \frac{\partial}{\partial x_j}\left[2\mu_m S_{ji} - \rho_m \overline{\boldsymbol{u'}_j \boldsymbol{u'}_i}\right] + \rho_m g_i \tag{2}$$

where α_l is the liquid volume fraction; $\overline{\boldsymbol{U}_i}$ and $\boldsymbol{u'}_i$ are the averaged mean and fluctuating velocity components respectively, ρ_m and μ_m are the volume-weighted density and viscosity respectively, P is the mean pressure, S_{ji} is the strain-rate tensor; the term $-\rho_m \overline{\boldsymbol{u'}_j \boldsymbol{u'}_i}$ represents the Reynolds stress tensor and $\rho_m g_i$ is the body force per unit volume. Mass and energy transfer between the phases were neglected. Surface tension effects are traditionally characterized by the Capillary number ($Ca = u_g \mu_l/\sigma$), representing the ratio of the viscous shear forces to the surface tension forces at the air-mucus interface [17]. The viscosity of mucus produced under diseased states is high, which adversely affects the role of surface tension resulting in $Ca \approx \mathcal{O}(10^2)$ [4]. Surface tension effects were thus considered to be negligible for our problem. A high-resolution scheme was used to solve the advection terms while a first order backward Euler scheme was used for the transient term. An anti-diffusive compressive discretization scheme was implemented to solve the advection of the volume fraction term [41]. The Reynolds stress term in the momentum equation was modeled using the $k-\omega$ shear stress transport (SST) turbulence model [43]. The $k-\omega$ SST model was chosen for our investigation considering its ability to provide accurate results in pulmonary [26,44,45] as well as multiphase flow studies [37,42].

A multi-block symmetric structured hexahedral mesh employing a butterfly topology [44] was generated using ANSYS® ICEM CFD™ (see Fig. 1(b)). The region around the interface was refined to capture the velocity gradients accurately. However, the location of the interface cannot be predicted *a priori* as it depends on the physical properties of the fluids, air-mucus interaction and the balance of forces, making the grid generation an intricate aspect of the investigation, particularly with the bifurcation models [26]. A separate grid independence study was performed for each geometry across three different grid resolutions (coarse, medium and fine) by successively refining the previous grid with approximately twice the number of elements. The results presented in this study for the sT, sBi, and dBi geometries were computed on the medium resolution grid consisting approximately 5×10^5, 9×10^5, and 1.3×10^6 elements, respectively. The grid resolution and the grid independence study performed using the grid convergence index approach proposed by Roache [46] are presented in Table 3. The non-dimensional wall distance (y^+) for the dry-wall models with airflow rates discussed earlier was < 1, while the mesh expansion ratio was maintained below 3. The time step for each iteration was calculated as a fraction of the ratio of inlet diameter to the mean air velocity. The solution convergence criteria were set at 10^{-4} for the residuals of individual variables and 1% for the global imbalance in the domain. Due to the unsteady nature of the interfacial waves, the simulations were continued for an additional 10^4 iterations by setting the convergence criteria to 10^{-5} for the residuals, and an averaging of the pseudo-transient solution was performed to achieve a quasi-steady state condition. Additional details regarding the numerical methods are presented in a supplementary document.

2.3. Validation with experimental results

The computational model and the results obtained were validated with the two-phase flow experiments carried out in a straight tube (sT) by Kim et al. [16]. Six experimental cases were

Table 3
Grid convergence study for two solution quantities: (a) mean tracheal mucus volume fraction, and (b) mean tracheal mucus velocity.

Geometry	Parameter	Coarse (1)	Medium (2)	Fine (3)
sT	N_x*	7/9	10/12	14/16
	N_y	7	10	14
	N_z	315	375	475
	N	220,500	*510,000*	1,223,600
	r	1.32**	1.34	
	(a) ε (%)/GCI (%)	3.36/5.61	1.97/3.11	
	(b) ε (%)/GCI (%)	6.51/10.87	3.84/6.06	
sBi	N_x*	6/12	9/16	12/20
	N_y	6	9	12
	N	403,416	*932,024*	2,175,744
	R	1.32**	1.33	
	(a) ε (%)/GCI (%)	4.52/7.56	2.71/4.46	
	(b) ε (%)/GCI (%)	6.65/11.12	3.96/6.52	
dBi	N_x*	6/12	8/16	11/20
	N_y	6	8	11
	N	565,416	1,306,*176*	3,089,664
	r	1.32**	1.33	
	(a) ε (%)/GCI (%)	5.08/8.42	2.82/4.59	
	(b) ε (%)/GCI (%)	8.52/14.11	4.76/7.74	

[Abbreviations: ($N_x \times N_y \times N_z$) – grid resolution, z being the axial/streamwise direction, N – total number of mesh elements; r – refinement factor; ε – relative error; GCI – grid convergence index].

* $\mathbf{N_x}$ is reported as number of elements in the core-region/wall-region. The core-region consists of 4 blocks while the wall-region consists of 8 blocks. Refer Plane 1 in Fig. 1(b) for clarity.

** Smaller of the r values used for calculations to check convergence towards asymptotic solution (refer supplementary document for more details).

selected (see Table 4), and the mean mucus layer thickness (h_l) and average mucus velocity (u_l) were compared (see Fig. 2). Assuming a uniform mucus layer lining the tube, the average thickness and velocity were calculated as:

$$h_l = \frac{D}{2}\left(1 - \sqrt{1-\alpha_l}\right); \quad u_l = J_l/\alpha_l \tag{3}$$

where D is the diameter of the tube, α_l and J_l are the volume-averaged mucus volume fraction and superficial velocity respectively. Based on the conservation of mass, the theoretical mucus layer velocity for an ideal annular flow is defined as $u_{th} = Q_l/(A_{OUT} \times \alpha_l)$, where A_{OUT} is the area at the outlet. On comparison with the experimental results, the computation of thickness and velocity were accurate within 2% and 4%, respectively, for all the cases as reported in Table 4. Due to the huge variation in the velocities between the phases, the 0.83 L/s airflow rate case required a finer grid and was solved on a mesh with 8×10^5 elements. The pressure drop data from the experiments of Kim et al. [16] is available only for the mucus viscosity of 200P; the computed values were higher (~30%) than that reported in the experiments. The pressure drop in a vertical annular flow depends on the balance between gravitational, interfacial shear, wall shear and acceleration forces [16]. The over-prediction of pressure drop in the current investigation can be related to the high velocity gradients at the untreated air-mucus interface resulting in higher turbulence generation thereby causing the velocity profile to be skewed [47]. However, additional experimental data is required to further reason and validate the computed pressure drop and serves as motivation for future experiments.

3. Results and discussion

The effect of mucus viscosity and airflow rates on mucus transport and distribution in a two-phase air-mucus flow is investigated. The flow structures developed in mucus-lined models are discussed.

3.1. Effect of mucus viscosity and airflow rate

The computational model used provides information regarding the flow morphology (concentric/eccentric core-annular) as well as on the turbulent nature of the waves and their amplitudes. The increase in mucus viscosity from 79P to 200P resulted in an increase in the mean layer thickness with a corresponding reduction in the mean layer velocity (see Table 4). On the contrary, increase in airflow rate from 0.33 L/s to 0.83 L/s, caused a successive increase in the mucus velocity and thinning of the mucus layer. These observations are consistent with previously reported experiments [16,17], and numerical models [8,22,48]. Mucus thickness (h) and velocity (u) were normalized using the average mucus thickness (h_l) and velocity (u_l) (reported in Table 4) to allow for comparison between the different test cases. The normalized thickness (h/h_l) ranged between 0.8 and 1.25 for all the cases considered which imply that the maximum wave amplitude $<0.03D$. Furthermore, the normalized velocity (u/u_l) was less than 3.2 for all the cases, while the higher viscosity lower flowrate case (sT-200P-0.33 L/s) had a value of less than 2.4. Fig. 3(a) plots the interfacial waves, normalized thickness and normalized velocity along the tube for sT-200P-0.5 L/s case. The experimental studies reported a relatively even mucus layer thickness in both longitudinal and circumferential directions by observing the advancing axisymmetric ring wave front as well as by measuring velocities at various locations across the tube [16,17]. Since the mucus feed rate is held constant, based on the continuity equation, the variation in velocity and thickness are directly related through the relation $u_l = \frac{4Q_l}{\pi D^2}[1-(1-\frac{2h_l}{D})^2]^{-1}$. Though the normalized thickness and velocity plotted along the length of the tube represent a strong correlation, there exist certain locations where they differ. A detailed analysis at one such location ($z/D = 5$) illustrates the presence of a larger amplitude wave upstream (at $z/D \approx 5.7$) resulting in the formation of vortices in front of the steep wave which reduces the interfacial drag, therefore explaining the uncoupled behavior. The mucus layer thickness and mucus velocity were averaged across a total of 1000 planes along the length of the tube. For all the sT cases, the distribution

Table 4
Comparison of computational results for a straight tube (sT) for a mucus feed rate (Q_l) of 1.67×10^{-5} L/s with experimental data from Kim et al. [16].

Case	Mucus viscosity, μ_l (P)	Airflow rate, Q_{air} (L/s)	Mean layer thickness, h_l (mm)			Mean layer velocity, u_l ($\times 10^{-4}$ m/s)		
			[a]Exp.	[b]CFD	% Error	[a]Exp.	[b]CFD	% Error
sT-79P-0.33 L/s	79	0.33	1.15	1.137	1.13	5.34	5.45	1.91
sT-79P-0.5 L/s	79	0.5	0.95	0.968	1.89	6.35	6.14	3.32
sT-79P-0.83 L/s[c]	79	0.83	0.76	0.746	1.84	8.02	8.33	3.92
sT-200P-0.33 L/s	200	0.33	1.38	1.395	1.09	4.68	4.85	3.63
sT-200P-0.5 L/s	200	0.5	1.11	1.105	0.45	5.18	5.37	3.71
sT-200P-0.83 L/s[c]	200	0.83	0.89	0.907	1.91	6.51	6.75	3.67

[a] The standard error in the experimental results are within 1% of the above reported experimental values [16].
[b] The mean mucus layer thickness and velocity are calculated using Eq. (3).
[c] The 0.83 L/s airflow rate cases were calculated on a finer mesh with 8×10^5 elements.

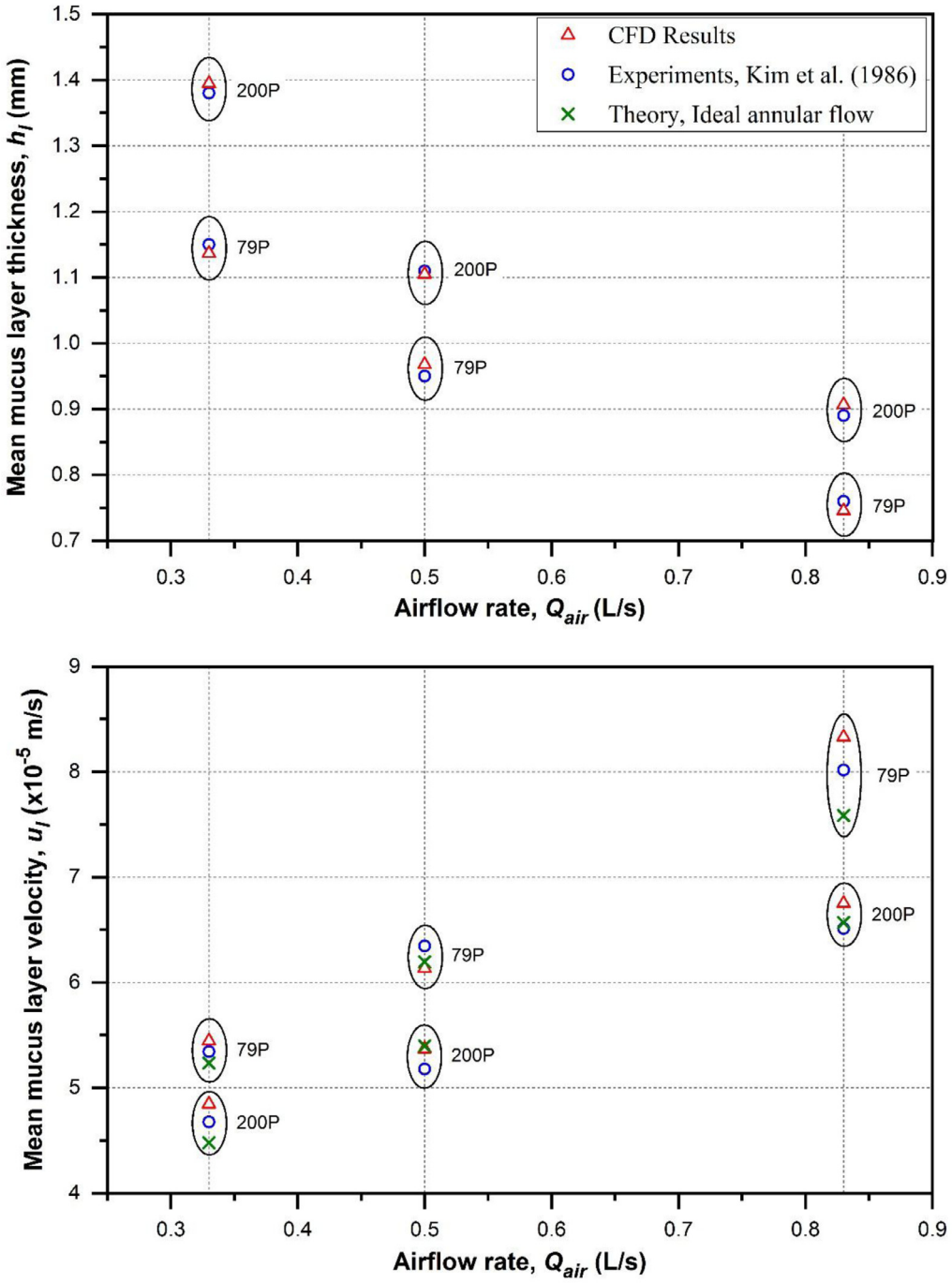

Fig. 2. (Online Color) Comparison of results from the current study with experimental data of Kim et al. [5] and theory based on mass conservation principles. Mean mucus layer thickness vs. airflow rate (a), and mean mucus layer velocity vs. airflow rate (b) are plotted. The vertical dotted lines represent airflow rates of 0.33, 0.5 and 0.83 L/s. Refer Table 3 for experimental and CFD data. Experimental data for an airflow rate of 1.17 L/s is available, however, it was not considered for the current investigation.

of the mucus layer thickness was symmetric, while the distribution of velocity was positively skewed (see Fig. 3(b)).

The mean mucus layer thickness and transport speed measured at the trachea are listed in Table 5. The mean layer thickness at the trachea for all the bifurcation cases was between 9.6 and 11.5% of the tracheal diameter. The interfacial distribution in the daughter branches could be classified as an eccentric-core annular regime with varying values of eccentricity depending on the inclination of the tube, mucus viscosity, and airflow rate. Mucus tends to remain along the inner-walls of the bifurcation forming a thicker layer with increased transport speed due to the higher interfacial drag [7,16]. The quantity of mucus along the inner-wall of G1 branch was 24%–36% more than the outer-wall for all the bifurcation cases. In the sBi models, mucus quantity along the inner and outer walls was highest for sBi-200P-0.9 L/s (higher viscosity, lower flowrate), and lowest for sBi-79P-1.2 L/s (lower viscosity, higher flowrate). The increase in viscosity from 79P to 200P, increased the mucus quantity along the inner-wall by 11%–14% whereas at the outer-wall it increased by 2.5%–6.5%. The increase in flowrate from 0.9 L/s to 1.2 L/s, decreased the mucus quantity along both the inner and outer walls by 7%–9.5% and 14.5%–17.7%, respectively. In the second bifurcation of the dBi models, the quantity of mucus along

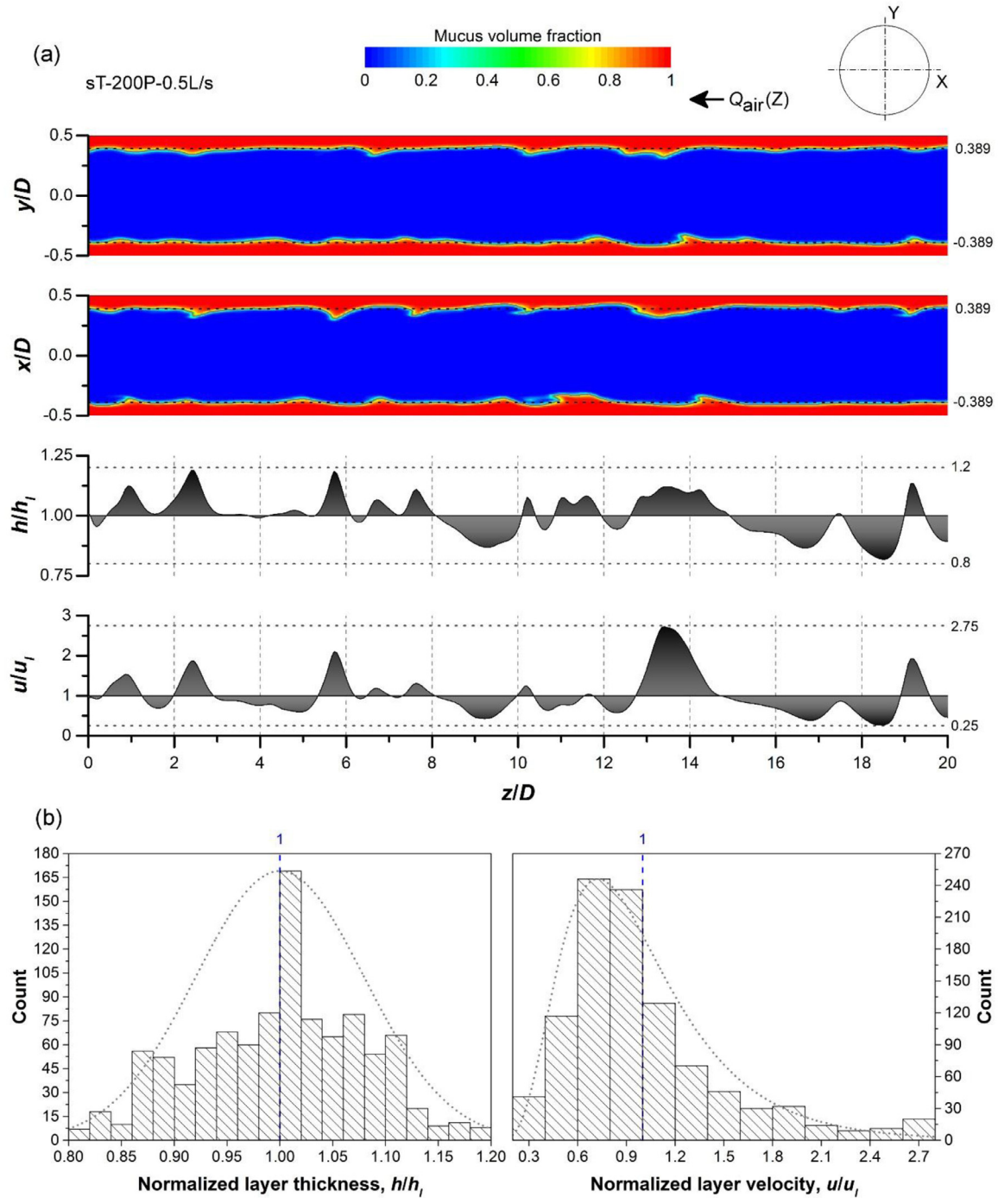

Fig. 3. (Online Color) (a) Mucus volume fraction contour plots at two cross sections (YZ and XZ), the normalized thickness, h/h_l and normalized velocity, u/u_l are plotted along the length of the tube for sT-200P-0.5 L/s case. The contour plot has been rotated counter-clockwise and scaled appropriately to fit data. (b) Distribution curve of the normalized thickness and velocity.

Table 5
Tracheal mucus layer thickness and velocity for the bifurcation cases for a mucus feed rate (Q_l) of 3.33×10^{-5} L/s. The tracheal diameter (D_T) = 16.4 mm.

Case	Mucus viscosity, μ_l (P)	Airflow rate, Q_{air} (L/s)	Mean layer thickness, h_l (mm)	Mean layer velocity, u_l ($\times 10^{-4}$ m/s)	h_l/D_T
sBi-79P-0.9 L/s	79	0.9	1.689	4.262	0.103
sBi-79P-1.2 L/s	79	1.2	1.577	4.638	0.096
sBi-200P-0.9 L/s	200	0.9	1.837	3.949	0.112
sBi-200P-1.2 L/s	200	1.2	1.666	4.374	0.102
dBi-79P-0.9 L/s	79	0.9	1.672	4.309	0.102
dBi-200P-0.9 L/s	200	0.9	1.827	3.973	0.111

the inner-wall was 33.2%–49.2% higher in G2-1 branch and 7%–8.5% lower in the G2-2 branch as compared to the outer-wall. The higher viscosity case dBi-200P-0.9 L/s formed a thicker lining analogous to the sT and sBi cases. It was also observed across all the bifurcation models that the mucus quantity along the outer-walls of the bifurcation was affected by the mucus viscosity due to the resistance offered to the circumferential motion of mucus, therefore resulting in lower eccentricity. Similarly, the quantity along the inner-walls was influenced by the airflow rate due to the increased interfacial shear. The analysis of the individual cases established that mucus quantity along the outer-walls of the G1 and G2-1 branches remained constant due to the absence of the large amplitude waves which is consistent with the observation of Sturm [49].

3.2. Flow structures in the bifurcation

The velocity at any location, at a cross-sectional plane along the flow field is composed of two components: (i) the axial or primary velocity; directed downstream along or parallel to the central axis of the branch and normal to the plane, and, (ii) the secondary velocity; which occurs perpendicular to centreline along the cross-sectional plane [50]. Secondary flow is developed when a fluid flows through a curved pipe and the centrifugal force acting on the fluid is balanced by a radial pressure gradient, which drives the faster-moving fluid towards the outer curvature and the slower-moving fluid towards the inner curvature of the pipe. Secondary flow is categorized as any flow that is superimposed on the bulk primary flow and it induces lateral mixing which determines gas transport and particle deposition [31].

3.2.1. Primary flow

The axial velocity vector plot of both air and mucus phases in the bifurcation plane for cases sBi-79P-0.9 L/s and dBi-79P-0.9 L/s are plotted and compared with their corresponding dry-wall (no mucus-lining) cases in Fig. 4. The characteristic bi-peaked velocity profile was observed in the parent branch which becomes fully developed downstream, while an asymmetric velocity profile was observed in the daughter branches as discussed by Evrensel et al. [23]. The increased interfacial shear acting on the thicker inner-wall mucus layer resulted in an increased mucus velocity (see Fig. 4). This is consistent with experimental results of Ragavan et al. [7], where they reported that a larger frontal area exposed to the flow generated a larger drag force, resulting in increased mucus displacement at higher angles of inclination. Kleinstreuer and Zhang [51] described that during expiration, while the basic flow features remain the same, a change in flowrate affects the axial distance of the merging location where the two daughter streams come together. This variation in the merging location is known to be caused by the interaction of convective acceleration and viscous effects near the wall. In the mucus-lined airways, the axial airflow from the two daughter branches merged further away from the carina when compared to a dry-wall model, and the merging location varied between 0.685D - 0.93D for the different cases studied. The cases sBi-79P-0.9 L/s and sBi-200P-1.2 L/s had a similar distribution of mucus along the inner and outer walls, and they merge at an axial distance of ~0.685D from the carina, illustrating the impact of mucus distribution on the merging location.

3.2.2. Secondary flow

The secondary flow strength (SFS) is defined as the area averaged ratio of radial velocity component to the axial velocity at a cross-sectional plane [30,45]. In the current study, mucus accumulates at locations close to the carina ($<0.5D$), which restricts the interaction of Dean vortices developed in the daughter branches. Sturm [49] and Manolidis et al. [4] also reported excessive accumulation of mucus at the carinal ridges due to increased mucus viscosity, impaired mucociliary clearance and local flow structures which is consistent with the conditions exercised in the current study. The thick mucus layer on top of the carina shifts the merging location of airstreams from the daughter branches downstream compared to the dry-wall model. As the airstreams from the daughter branches merge in the parent branch, secondary flow structures are established, resulting in an increase in SFS and a corresponding decrease in the mucus volume fraction. Fig. 5 compares the secondary velocity vector and axial velocity contour plot overlaid with the air-mucus interface at five locations: Planes A–A and B–B along the daughter branches near the carina; Planes C–C, D–D, and E–E at a streamwise distance of 0.65D, 1.15D, and 1.65D respectively from the carina for the case sBi-79P-0.9 L/s with the corresponding dry-wall case. At both A–A and B–B, a single pair of Dean vortices are established due to the curved section of the flow divider. The direction of rotation of the vortices illustrate that the slower-moving air is driven towards the inner-side of the bend along the central plane while the faster-moving air is pushed to the outer-side of the bend along the top and bottom. At C–C, the airflow from the daughter branches merges towards the center of the parent branch, whereas two pairs of symmetric counter-rotating vortices are set for the dry-wall case. At D–D, a bi-peaked axial velocity profile with four counter-rotating vortices can be noticed for the mucus-lined case. However, they are asymmetric due to the presence of waves on the mucus surface. At E–E, the velocity profile of air reaches near its fully developed state for the mucus-lined case whereas the bi-peaked profile was observed in the dry-wall case in addition to a weaker secondary flow in both the cases. The intensity of secondary flow for the both the cases slowly decreases along the trachea. The direction of rotation of the vortices are an indication of the two daughter flow streams proceeding towards the center of the parent branch in the bifurcation plane and away from the center in the transverse plane [34].

Fig. 6(a) plots the normalized secondary velocity at transverse planes A'–A' and B'–B' for dBi-79P-0.9 L/s. The plots represent the regions of peak SFS in G0 and G1 branches which are comparable with the sBi cases. The peak SFS for dBi-79P-0.9 L/s was at 1.1D from the carina while it moved downstream to 1.56D from the carina for dBi-200P-0.9 L/s. Fig. 6(b) represents the secondary velocity vector and the axial velocity contour plot overlaid with the air-mucus interface at two locations as indicated in the schematic. At D'–D', which is located 1.15D from the carina, four asymmetric counter-rotating vortices were observed for both the cases similar to the sBi cases. Adler and Brücker [52] reported that irrespective of asymmetric flow structures in the lower generations, the flow features in the trachea remain the same, which holds true for the mucus-lined cases. At the cross-section of peak SFS in the generation G1 parent tube, four asymmetric counter-rotating vortices were noticed. However, they were skewed towards the outer-wall as the axial velocity of the flow from the two daughter branches (generation G2-1 and G2-2) was different. The peak axial velocity was greater for the air stream from generation G2-2 branch compared to G2-1. At C'–C' (entrance of the curved bifurcation region), the vortices become weaker, and as it passes through the curvature, a single pair of vortices appears analogous to the dry-wall case. When the axial velocity is identical, the flow from the daughter branches converges towards the center at the same rate and merges exactly at the center of the parent tube. However, when the velocities are different, they converge towards the center at a different rate, resulting in a skewed velocity profile. The decrease in mucus volume fraction at the flow divider region was observed with the dBi cases analogous to the sBi cases. This indicates that drug particles deposited on flow divider regions throughout the respiratory tract have a greater potential to be absorbed into the

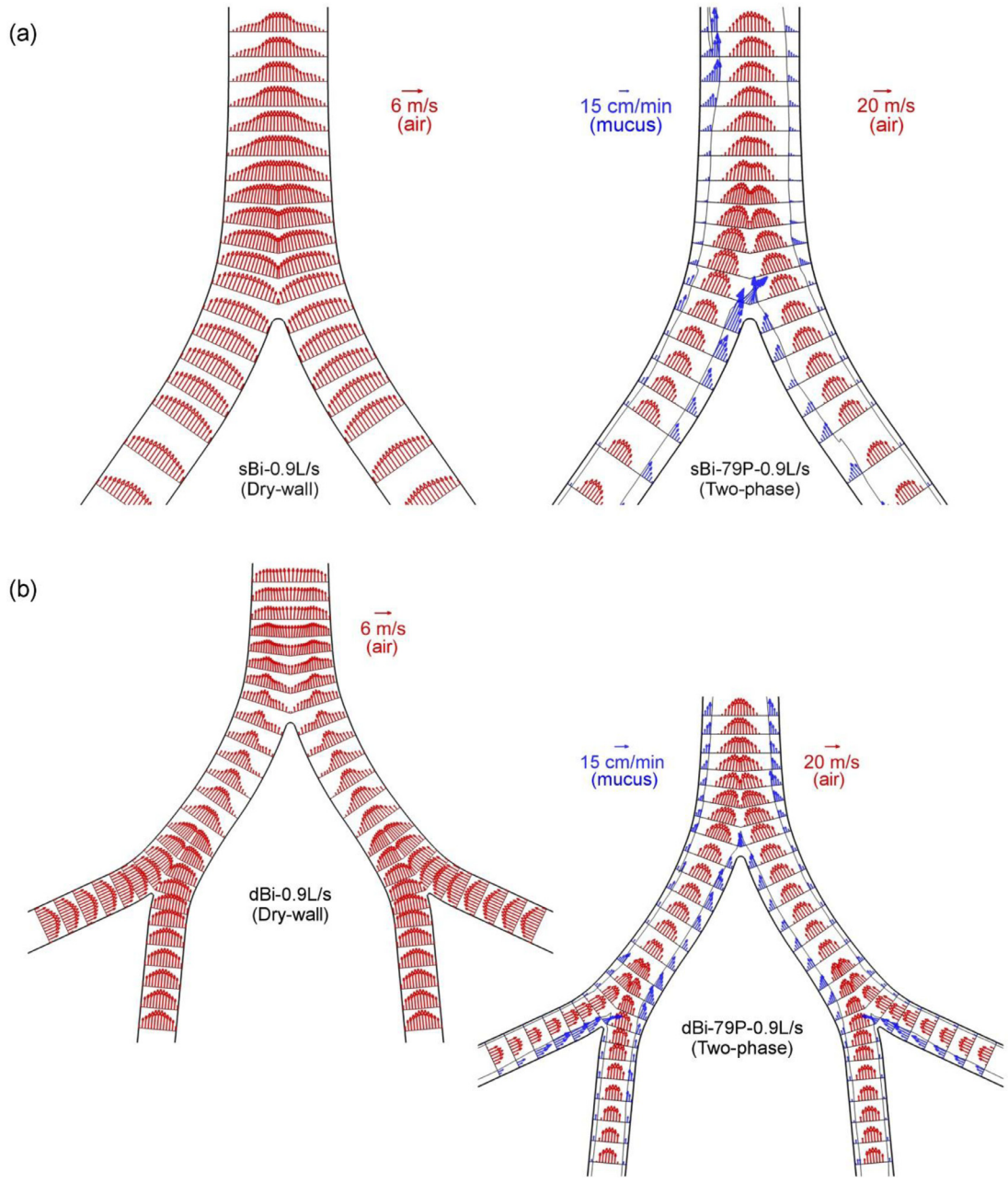

Fig. 4. (Online Color) (a) Axial velocity vector plot at bifurcation plane for the dry wall sBi case and the mucus-lined sBi case (sBi-79P-0.9 L/s). (b) Axial velocity vector plot for the dry wall dBi case and the mucus-lined dBi case (dBi-79P-0.9 L/s). The airflow is represented by red vectors and the annular mucus by blue vectors. (For interpretation of the references to color in this figure legend, the reader is referred to the web version of this article.)

systemic circulation than being cleared. However, due to the difference in the axial velocity of the G2 daughter branches merging at the G1 parent flow divider region, the mucus volume fraction drop was observed at two locations, 0.1D apart from each other, illustrating that mucus distribution is uneven and discontinuous throughout the airway tree.

3.3. Effect of gravity and geometry

The effect of gravity in the larger airways cannot be ignored in pathological cases where a thick mucus layer is formed [5,8,53]. The angle of inclination, θ, is defined as the angle between the central axis of the daughter airway and the direction of gravity. The inclination angles of the G1, G2-1, and G2-2 daughter branches of the bifurcation models are 35°, 65°, and 5° respectively. As the angle of inclination increases, less resistance is offered to the flow causing increased mucus velocities as reported in horizontal and downward inclinations [7,11]; a secondary mucus velocity is developed which is directed towards the inner-wall resulting in an increased mucus layer thickness. Furthermore, the flow morphology transitions from a gravity-dominated eccentric core-annular flow with the core skewed towards the outer-wall, into a thick stratified mucus layer at the bottom of the branch at near horizontal inclinations [11,16]. Fig. 7(a) shows the effect of gravity at two locations: Planes 1–1 and 2–2 for sBi-79P-0.9 L/s case, where the secondary velocity of mucus is directed towards the inner-wall

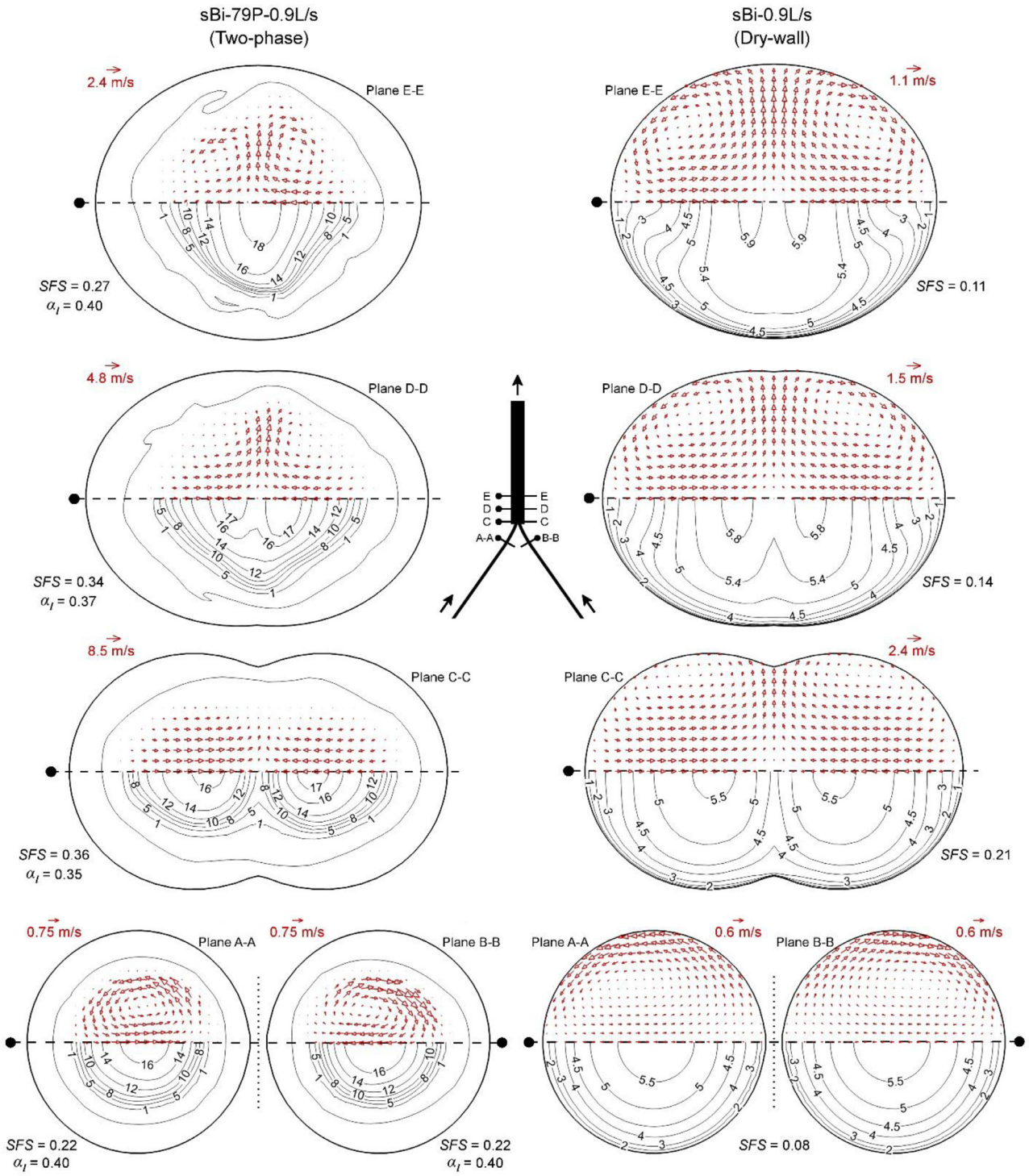

Fig. 5. (Online Color) Comparison of flow structures at five different planes near the carina of case sBi-79P-0.9 L/s (left) with the corresponding dry-wall case sBi-0.9 L/s (right). Planes A–A and B-B exist along the daughter branch while planes C–C, D–D and E-E lie along the parent branch at 0.65*D*, 1.15*D* and 1.65*D* from the carina. The plot shows the secondary velocity vector plot on the top - axial velocity contour at the bottom and both overlaid alongside the air-mucus interface location. The axial velocity is oriented into the page.

forming a thicker mucus layer compared to the outer-wall. The thickness of the mucus layer at the inner-wall depends on the mucus secondary flow, which is promoted by the angle of inclination and resisted by the mucus viscosity in addition to the airflow induced interfacial drag. Therefore, the gravitational force, depending on the orientation of the individual branches, may possibly enhance mucus clearance from the airways [16,54]. However, at an upright body position, gravity invariably hinders mucus transport in the trachea and first few generations, which has been considered in the current study.

Fig. 7(b) illustrates the effect of centrifugal forces in reversing the direction of mucus secondary flow, from moving towards the inner-wall of the bifurcation to moving away from it, at two planes; the start (Plane 3–3) and end (Plane 4–4) of the curved

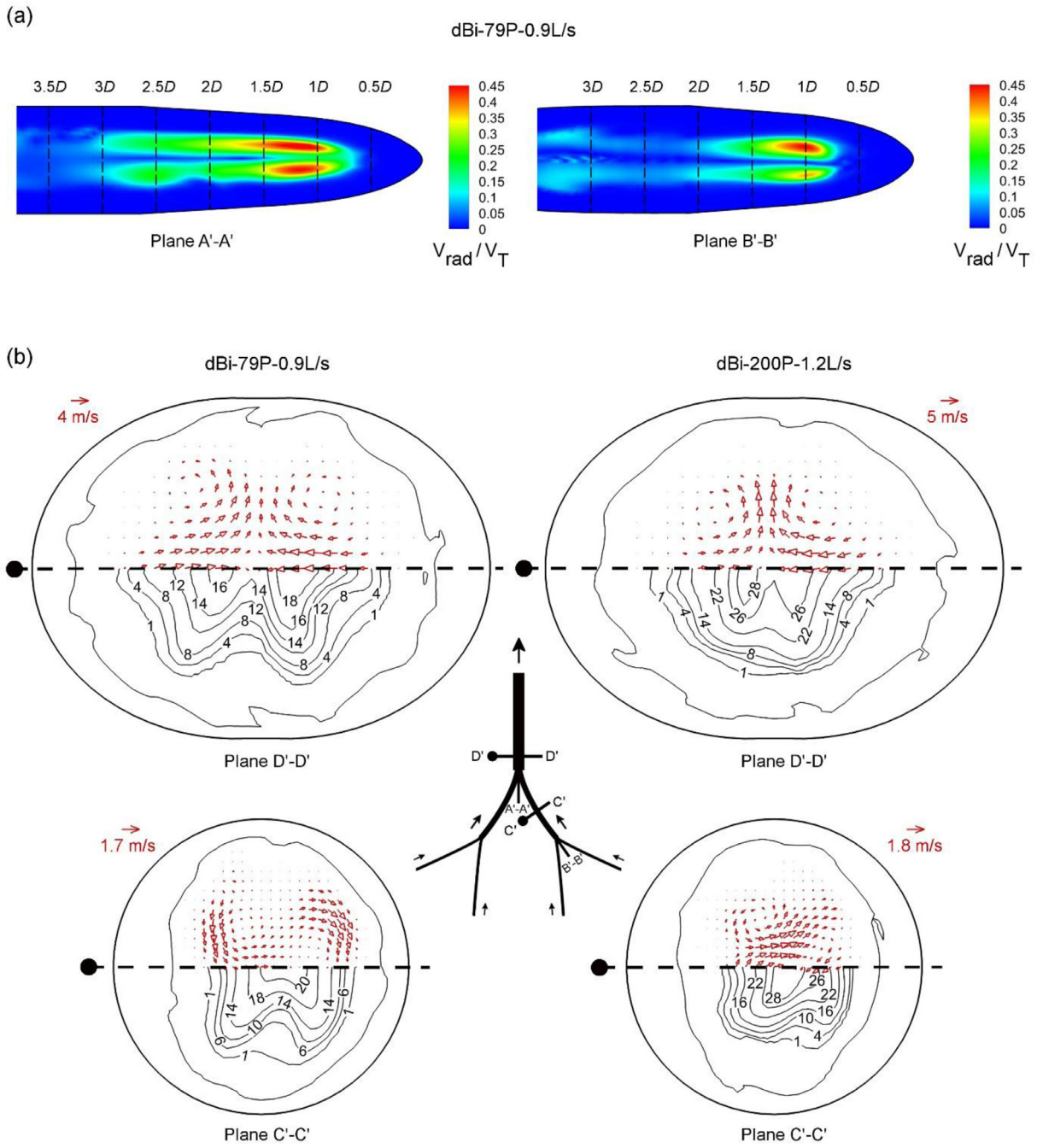

Fig. 6. (Online Color) (a) Secondary velocity contour for dBi-79P-0.9 L/s indicating region of maximum SFS at transverse planes A'–A' (1st bifurcation) and B'–B' (2nd bifurcation); distances represented from the bifurcation location, (b) The plot highlights the secondary velocity vector plot on the top - axial velocity contour at the bottom and both overlaid alongside the air-mucus interface location for the two dBi cases at planes C'–C' and D'–D'. The axial velocity is oriented into the page. *D* is the diameter of the parent branch where the daughter streams merge.

flow divider section for sBi-79P-0.9 L/s case. When a two-phase gas-liquid flow enters a curved pipe, the centrifugal force usually moves the denser-liquid towards the outer-wall of the bend resulting in increased liquid thickness [37,40]. However, in the air-mucus flow under consideration, the ratio of air to mucus velocity is $\mathcal{O}(10^4)$ and thus the momentum flux of air is much greater than that of the mucus, $\mathcal{O}(10^6)$. Therefore, the airflow moves towards the central axis from an eccentric-core to a concentric-core configuration and drives the denser mucus towards the inner-wall of the bend. This phenomenon is known as film inversion and has been reported in curved pipes [55]. It is to be noted that the inner-wall of the bend/curvature is the same as the outer-wall of the bifurcation. For all the bifurcation cases at generation G1, the degree of eccentric core-annular flow along the curved flow divider region decreased by more than 60%. The eccentricity was least for sBi-200P-0.9 L/s case (high viscosity-low flowrate) where it decreased from 19.2% to 2.3%; while it was highest for sBi-79P-1.2 L/s case (low viscosity-high flowrate) where it decreased from 75.1% to 29.2%. Therefore, the centrifugal force causes a local redistribution of mucus along the curved region to reduce the eccentricity, potentially increasing the aerosol deposition along the inner-wall of the curvature.

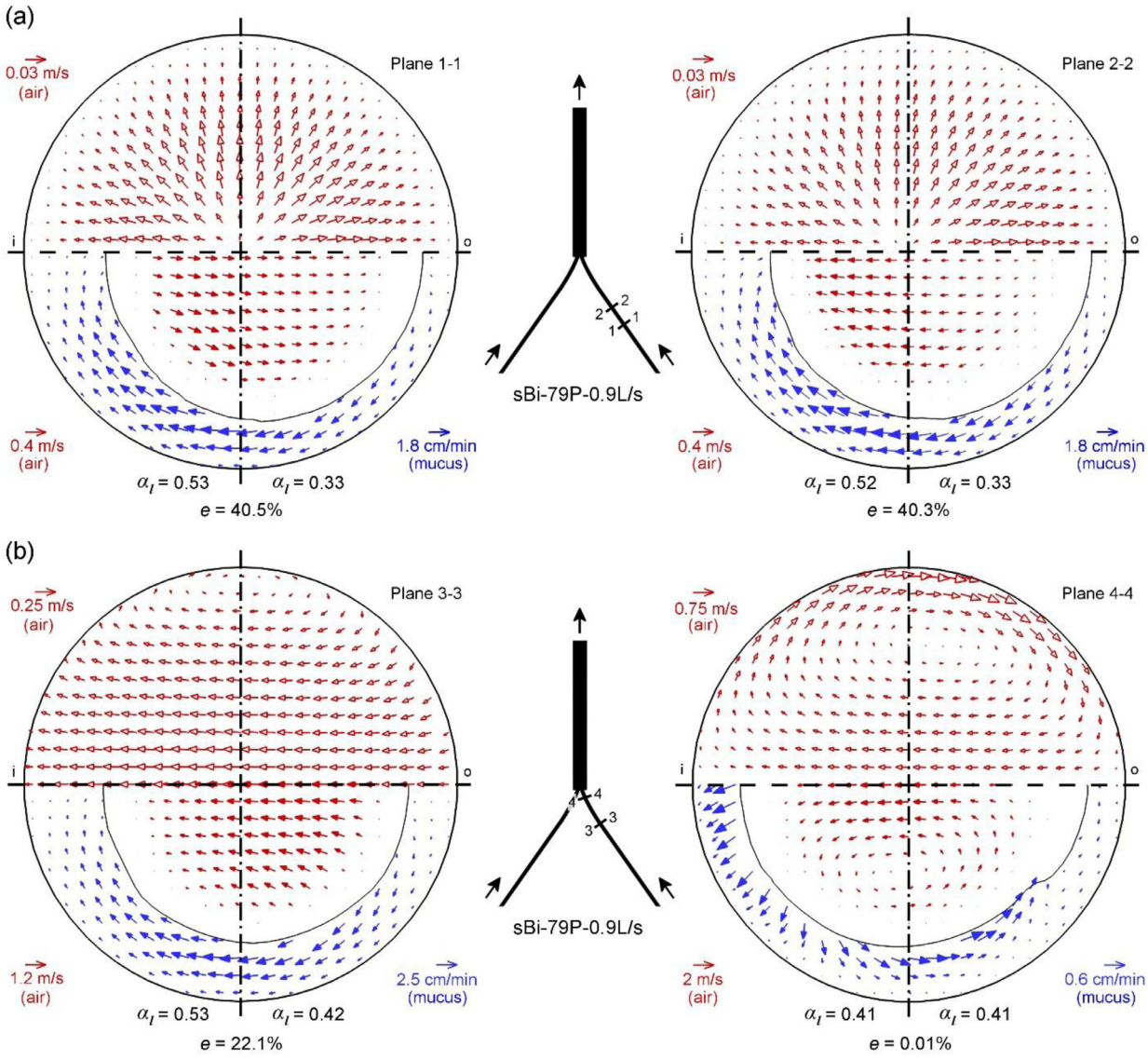

Fig. 7. (Online Color) Secondary flow in the sBi-79P-0.9 L/s (bottom-half) and dry wall case (top-half). (a) The effect of gravity at two planes (Plane 1–1 & Plane 2–2) along the daughter branch where the mucus secondary velocity is directed towards the inner wall resulting in a thicker mucus layer; (b) The effect of geometry illustrated at two planes (3–3 & 4–4) along the "curved section" of the flow divider region. The eccentricity of the core-annular flow reduces due to the centrifugal effects. The airflow is represented by red vectors and the annular mucus by blue vectors. Abbreviations: α_l is the mucus volume fraction area-averaged over the semi-circular regions along the inner and outer walls; *e* - eccentricity; *o* - outer wall of the bifurcation; *i* - inner wall of the bifurcation. (For interpretation of the references to color in this figure legend, the reader is referred to the web version of this article.)

The optimal site for drug therapy in the airway tree depends on the type and severity of the disease (local or systemic) being treated [9]. The thicker mucus layer serves as a potential site for drug delivery targeted towards improving clearance, while the thinner mucus layer exhibits a greater potential of the drug being absorbed into systemic circulation. However, due to increased mucus accumulation, deposition would occur predominantly in the central airways hindering drug penetration to the distal airway regions. Furthermore, obstruction caused by uneven mucus accumulation results in the inhaled drugs being diverted away from the regions of obstruction thereby reducing the therapeutic effect. Similarly, chest physiotherapy improves mucus clearance by controlled coughing and breathing exercises, however, high airflow rates increase patient discomfort. The overall effectiveness of therapy can be improved by analyzing the distribution of mucus in the airway tree at various viscosities and airflow rates which assists in selecting the appropriate particle size distribution capable of reaching the obstructed airways and devising a tailored breathing maneuver that would minimize discomfort.

4. Conclusions

A CFD study on two-phase air mucus flow under steady expiration was conducted in idealized lung models. The primary focus of the investigation was to understand the role of expiratory airflow in mucus distribution and clearance and to identify the flow structures in the mucus-lined airways. The following conclusions were made. An increase in viscosity resulted in a thicker mucus layer with lower mucus velocity in the vertical sections of the geometry. However, an increase in the airflow rate resulted in a thinner layer with higher mucus velocity. Both these findings were consistent with experimental data available in the literature. The uneven distribution of the mucus along the inner and outer walls of the bifurcation models affected the merging location of the airflow from the daughter branches, thereby influencing the lateral

mixing that occurs due to secondary flows. The region of high secondary flow strength in all the cases studied corresponded with a drop in the mucus volume fraction across the parent branch of the flow divider. The inner-wall mucus layer thickness in the inclined daughter branches was influenced by the mucus secondary flow. A higher angle of inclination from the vertical increases the mucus secondary flow while mucus viscosity and airflow rate oppose it. The centrifugal force acts to decrease the eccentricity of the core-annular flow by circumferentially redistributing the mucus from the inner-wall towards the outer-wall of the bifurcation as the flow enters the curved section of the geometry.

Acknowledgment

The authors would like to thank Mohammed Alzahrany for various suggestions and insightful thoughts on the current work.

Competing interests

None declared.

Funding

None.

Ethical approval

Not required.

Supplementary materials

Supplementary material associated with this article can be found, in the online version, at doi:10.1016/j.medengphy.2019.02.006.

References

[1] Fahy JV, Dickey BF. Airway mucus function and dysfunction. N Engl J Med 2010;363:2233–47.
[2] Mitran S. Continuum-kinetic-microscopic model of lung clearance due to core-annular fluid entrainment. J Comput Phys 2013;244:193–211.
[3] Samet JM, Cheng PW. The role of airway mucus in pulmonary toxicology. Environ Health Perspect 1994;102:89–103.
[4] Manolidis M, Isabey D, Louis B, Grotberg JB, Filoche M. A macroscopic model for simulating the mucociliary clearance in a bronchial bifurcation: the role of surface tension. J Biomech Eng 2016;138:121005.
[5] van der Schans CP, Postma DS, Koeter GH, Rubin BK. Physiotherapy and bronchial mucus transport. Eur Respir J 1999;13:1477–86.
[6] Levy R, Hill DB, Forest MG, Grotberg JB. Pulmonary fluid flow challenges for experimental and mathematical modeling. Integr Comp Biol 2014;54:985–1000.
[7] Ragavan AJ, Evrensel CA, Krumpe P. Interactions of airflow oscillation, tracheal inclination, and mucus elasticity significantly improve simulated cough clearance. Chest 2010;137:355–61.
[8] Mauroy B, Fausser C, Pelca D, Merckx J, Flaud P. Toward the modeling of mucus draining from the human lung: role of the geometry of the airway tree. Phys Biol 2011;8:056006.
[9] Labiris NR, Dolovich MB. Pulmonary drug delivery. Part I: physiological factors affecting therapeutic effectiveness of aerosolized medications. Br J Clin Pharmacol 2003;56:588–99.
[10] Coleman JW, Garimella S. Characterization of two-phase flow patterns in small diameter round and rectangular tubes. Int J Heat Mass Transf 1999;42:2869–81.
[11] Hanratty TJ. Physics of gas-liquid flows. Cambridge: Cambridge University Press; 2013.
[12] Kim CS, Brown LK, Lewars GG, Sackner MA. Deposition of aerosol particles and flow resistance in mathematical and experimental airway models. J Appl Physiol 1983;55:154–63.
[13] Kim CS, Eldridge MA. Aerosol deposition in the airway model with excessive mucus secretions. J Appl Physiol 1985;59:1766–72.
[14] King M, Brock G, Lundell C. Clearance of mucus by simulated cough. J Appl Physiol 1985;58:1776–82.
[15] Kim CS, Eldridge MA, Rodriguez CR, Sackner MA. Criteria for mucus transport in the airways by two-phase gas-liquid flow mechanism. J Appl Physiol 1986;60:901–7.
[16] Kim CS, Greene MA, Sankaran S, Sackner MA. Mucus transport in the airways by two-phase gas-liquid flow mechanism: continuous flow model. J Appl Physiol 1986;60:908–17.
[17] Camassa R, Forest MG, Lee L, Ogrosky HR, Olander J. Ring waves as a mass transport mechanism in air-driven core-annular flows. Phys Rev E Stat Nonlinear Soft Matter Phys 2012;86:066305.
[18] Chang HK, Weber ME, King M. Mucus transport by high-frequency nonsymmetrical oscillatory air-flow. J Appl Physiol 1988;65:1203–9.
[19] Kim CS, Iglesias AJ, Sackner MA. Mucus clearance by two-phase gas-liquid flow mechanism: asymmetric periodic flow model. J Appl Physiol 1987;62:959–71.
[20] Zahm JM, King M, Duvivier C, Pierrot D, Girod S, Puchelle E. Role of simulated repetitive coughing in mucus clearance. Eur Respir J 1991;4:311–15.
[21] Evrensel CA, Khan RU, Krumpe PE. Response of a viscoelastic layer (mucus) to turbulent airflow in a rigid tube. Technol Health Care 2008;16:355–66.
[22] Evrensel CA, Khan MR. Interaction of laminar airflow with viscoelastic airway mucus. Technol Health Care 2003;11:149–59.
[23] Evrensel CA, Khan RU, Elli S, Krumpe PE. Viscous airflow through a rigid tube with a compliant lining: a simple model for the air-mucus interaction in pulmonary airways. J Biomech Eng 1993;115:262–70.
[24] Satpathi DK, Ramu A. A laminar flow model for mucous gel transport in a cough machine simulating trachea: effect of surfactant as a sol phase layer. Open J Appl Sci 2013;04:6 Vol.03No.
[25] Leith DE, Butler JP, Sneddon SL, Brain JD. Cough. Comprehensive physiology. John Wiley & Sons, Inc.; 2011.
[26] Paz C, Suárez E, Vence J. CFD transient simulation of the cough clearance process using an Eulerian wall film model. Comput Methods Biomech Biomed Eng 2017;20:142–52.
[27] King M. Physiology of mucus clearance. Paediatr Respir Rev 2006;7:S212–S2S4.
[28] Alzahrany M, Banerjee A. Aerosolized drug delivery in patient-specific lung model during invasive high frequency oscillatory ventilation. J Aerosol Sci 2015;81:1–20.
[29] Van Rhein T, Alzahrany M, Banerjee A, Salzman G. Fluid flow and particle transport in mechanically ventilated airways. Part I. Fluid flow structures. Med Biol Eng Comput 2015;54:1085–96.
[30] Alzahrany M, Banerjee A, Salzman G. Flow transport and gas mixing during invasive high frequency oscillatory ventilation. Med Eng Phys 2014;36:647–58.
[31] Zhao Y, Lieber B. Steady inspiratory flow in a model symmetric bifurcation. J Biomech Eng 1994;116:488–96.
[32] Weibel ER. Morphometry of the human lung. Berlin: Springer; 1963.
[33] Horsfield K, Dart G, Olson DE, Filley GF, Cumming G. Models of the human bronchial tree. J Appl Physiol 1971;31:207–17.
[34] Fresconi FE, Prasad AK. Secondary velocity fields in the conducting airways of the human lung. J Biomech Eng 2007;129:722–32.
[35] Thiruvengadam M, Armaly BF, Drallmeier JA. Shear-driven liquid film in a duct. Eng Appl Comput Fluid Mech 2009;3:506–13.
[36] De Schepper SCK, Heynderickx GJ, Marin GB. CFD modeling of all gas-liquid and vapor-liquid flow regimes predicted by the Baker chart. Chem Eng J 2008;138:349–57.
[37] El-Batsh HM, Doheim MA, Hassan AF. On the application of mixture model for two-phase flow induced corrosion in a complex pipeline configuration. Appl Math Model 2012;36:5686–99.
[38] Ghosh S, Das G, Das PK. Simulation of core annular downflow through CFD—A comprehensive study. Chem Eng Process Proc Intensif 2010;49:1222–8.
[39] Hirt CW, Nichols BD. Volume of fluid (VOF) method for the dynamics of free boundaries. J Comput Phys 1981;39:201–25.
[40] Zahedi P, Zhang J, Arabnejad H, McLaury BS, Shirazi SA. CFD simulation of multiphase flows and erosion predictions under annular flow and low liquid loading conditions. Wear 2017;376–377:1260–70.
[41] Zwart PJ. Numerical modelling of free surface and cavitating flows. In: Proceedings of the industrial two-phase flow CFD; 2005 von Karman Institute Lecture Series 2005-04. ISBN 2930389605.
[42] Haque JN, Mahmud T, Roberts KJ, Rhodes D. Modeling turbulent flows with free-surface in unbaffled agitated vessels. Ind Eng Chem Res 2006;45:2881–91.
[43] Menter FR, Kuntz M, Langtry RB. Ten years of industrial experience with the SST turbulence model. In: Hanjalic K, Nagano Y, Tummers M, editors. Turbulence, heat and mass transfer 4. Begell House, Inc.; 2003. p. 625–32.
[44] Longest PW, Vinchurkar S. Effects of mesh style and grid convergence on particle deposition in bifurcating airway models with comparisons to experimental data. Med Eng Phys 2007;29:350–66.
[45] Zhang Z, Kleinstreuer C. Computational analysis of airflow and nanoparticle deposition in a combined nasal–oral–tracheobronchial airway model. J Aerosol Sci 2011;42:174–94.
[46] Roache PJ. Perspective - a method for uniform reporting of grid refinement studies. J Fluid Eng T ASME 1994;116:405–13.
[47] Lo S, Tomasello A. Recent progress in CFD modelling of multiphase flow in horizontal and near-horizontal pipes. In: 7th North American conference on multiphase technology; 2010. p. 209–19.
[48] Satpathi DK, Kumar BVR, Chandra P. Unsteady-state laminar flow of viscoelastic gel and air in a channel: application to mucus transport in a cough machine simulating trachea. Math Comput Model 2003;38:63–75.
[49] Sturm R. Modeling the delay of mucous flow at the carinal ridges of the human tracheobronchial tree. Comput Math Biol 2014;6:1–13.
[50] Guha A, Pradhan K. Secondary motion in three-dimensional branching networks. Phys Fluids 2017;29:063602.
[51] Kleinstreuer C, Zhang Z. Airflow and particle transport in the human respiratory system. Ann Rev Fluid Mech 2010;42:301–34.

[52] Adler K, Brücker C. Dynamic flow in a realistic model of the upper human lung airways. Exp Fluids 2007;43:411–23.
[53] Song Y, Baudoin M, Manneville P, Baroud CN. The air–liquid flow in a microfluidic airway tree. Med Eng Phys 2011;33:849–56.
[54] Blake J. On the movement of mucus in the lung. J Biomech 1975;8:179–90.
[55] Abdulkadir M, Zhao D, Azzi A, Lowndes IS, Azzopardi BJ. Two-phase air–water flow through a large diameter vertical 180o return bend. Chem Eng Sci 2012;79:138–52.